The Resistance of Cu Nanowire-Nanowire Junctions & Electro-Optical Modeling of Cu Nanowire Networks

Hugh G. Manning,[1,2, a)] Patrick F. Flowers,[3] Mutya A. Cruz,[3] Claudia Gomes da Rocha,[4] Colin O' Callaghan,[5] Mauro S. Ferreira,[2,5] Benjamin J. Wiley,[3] and John J. Boland [1,2]

[1] *School of Chemistry, Trinity College Dublin, Dublin 2, Ireland.*

[2] *Advanced Materials and Bioengineering Research (AMBER) Centre, Trinity College Dublin, Dublin 2, Ireland.*

[3] *Department of Chemistry, Duke University, Durham, North Carolina, NC 27708-0354, USA.*

[4] *Department of Physics and Astronomy, University of Calgary,2500 University Drive NW, Calgary, Alberta T2N 1N4, Canada.*

[5] *School of Physics, Trinity College Dublin, Dublin 2, Ireland.*

[a)] Author to whom correspondence should be addressed. Electronic mail: manninh@tcd.ie

Abstract

Flexible transparent conductors made from networks of metallic nanowires are a potential replacement for conventional, non-flexible, transparent conducting materials such as indium tin oxide. Cu nanowires are particularly interesting as a cost-effective alternative to Ag nanowires– the most investigated metallic nanowire to date. To optimize the conductivity of Cu nanowire networks, the resistance contributions from the material and nanowire junctions must be independently known. In this paper, we report the resistivity values (ρ) of individual solution grown Cu nanowires $\langle\rho\rangle$ = 20.1 ± 1.3 nΩ·m and the junction resistance (R_{jxn}) between two overlapping Cu nanowires $\langle R_{jxn}\rangle$ = 205.7 ± 57.7 Ω. This electrical data is incorporated into an electro-optical model which generates analogs for Cu nanowire networks, that accurately predict without the use of fitting factors the optical transmittance and sheet resistance of the transparent electrode. The model's predictions are validated using experimental data from the literature of Cu nanowire networks comprised of a wide range of aspect ratios (nanowire length/diameter). The separation of the material resistance and the junction resistance allows the effectiveness of post-deposition processing methods to be evaluated, aiding research and industry groups in adopting a materials-by-design approach.

Metallic nanowire networks (NWN) provide a route to highly transparent, highly conductive, flexible, easy-to-fabricate and low-cost materials.[1] The large-scale integration of these materials in commercial devices could revolutionize display, touch screen, as well as numerous emerging applications.[2] To assess the true potential of metallic NWN systems, it is crucial to establish a complete understanding of their individual physical properties and how these properties affect the performance of the network.[3] This requires a part-to-whole consideration of the network, evaluating and characterizing each aspect of the system, such as the ability of the nanowire (NW) to conduct electrical charge and the electrical resistance at each of the NW junctions within the network. While Ag NWNs have their merits, the high-cost, susceptibility to corrosion and the potential future scarcity of Ag could prohibit their widespread adoption.[4] On the other hand, Cu in bulk form is only 6 % less conductive than Ag but 1500 times more abundant and 87 times cheaper.[5] Over the past number of years there has been a large amount of interest in using Cu NWs in composite materials and conducting networks.[6] Cu NWs are also promising candidates as interconnects in future nanodevices.[7] While the study of Cu NWNs is much less developed than their Ag counterparts, recent developments in Cu NW synthesis have allowed NWs with aspect ratios (length / diameter) as high as 5700 to be grown, that has allowed the fabrication of flexible transparent conductors with sheet resistance (R_s) performances of 50 Ω/□ at 90 % optical transmittance (T), making them a viable alternative to Ag NWNs.[8]

The performance of any network is not just dependent on the materials used but how the network is processed; this influences the properties of the nanowires and the junctions that comprise the network. The resistance of Ag NW junctions has been previously established,[9,10] and has enabled the comparison of post-processing conditions which remove the insulating polymer coating from the polyol synthesis method, and assisted in the development of accurate computational models predicting the performance of Ag NWN-based materials.[11,12] One drawback to Cu NWs is that they readily oxidize in ambient conditions, insulating the conducting core and causing a large contact resistance at each of the nanowire-nanowire junctions. Post-processing methods have been developed to remove the oxide layer, which include, acetic acid washes, plasma cleaning, high-temperature hydrogen annealing, and photonic welding.[13,14]

In this paper, we present the electrical measurements of solution grown Cu NWs, allowing the determination of the material resistivity (ρ) and junction resistance (R_{jxn}). Electrical

characterization of these fundamental material properties enables the use of a multi-nodal representation (MNR) electro-optical computational model to predict the R_s and T as a function of the R_{jxn}. Exploiting the electrical properties of individual Cu NWs and their junctions enables efficient comparison, optimization, benchmarking, and modelling of the corresponding NWN material.

Pentagonally twinned Cu NWs were synthesized using the method described by Rathmell et al.[15] To remove the Polyvinylpyrrolidone (PVP) and Diethylhydroxylamine (DEHA), the NWs were transferred into a volatile solvent using the following protocol. Disperse the NWs by shaking. Take a sample of the NWs, centrifuge at 2000 RPM for 3 mins and remove the supernatant. Using a 1 wt% DEHA solution the NWs were rinsed three times to remove the PVP. The NWs were rinsed with ethanol (EtOH) to remove the water and DEHA. NWs were then rinsed with isopropyl alcohol (IPA) to remove the EtOH. Finally, the NWs were suspended in IPA at the desired concentration. FIG. S1 presents transmission electron microscopy (TEM) analysis of the Cu NWs showing what appear to be stacking faults and a native oxide coating with noticeable surface roughness. FIG. S1 also details distributions of length (20.2 ± 12.5 μm), diameter (84 ± 18 nm), and the diameter dependent native oxide which forms on the surface of the wire. No significant length – diameter correlation was observed (FIG. S2).

Experiments were carried out on p-type silicon wafers (University Wafer) with a 300 nm thermally grown SiO_2 layer; the Cu NW solution was drop-cast onto substrates pre-patterned by UV lithography. Single and crossed Cu NWs were fabricated by electron-beam lithography (EBL) using previously reported techniques with 120 nm of electron beam evaporated Ag as the electrode material.[9] Scanning electron microscopy (SEM) imaging and EBL was performed using a Zeiss Supra FEG-SEM. TEM images were acquired using a FEI TITAN TEM. Electrical measurements were taken in ambient conditions on a Keithley 4200 SCS.

MNR simulations were carried out by solving Kirchhoff's circuit equations numerically. The model and the code is described in detail and is available in an earlier publication.[11] For predicting the performance of Cu NWNs, the material resistivity was set at ρ = 20.1 nΩm, while R_{jxn} was varied according to experiment. The extinction cross section, C_{ext}, was calculated using the MatScat (Mie theory for infinite cylinders) implementation by Schäfer *et al.*[16] using various values for NW diameter and the optical constants for Cu, n = 1.0344, k = 2.57984 at λ = 546 nm.[17] C_{ext} is transformed into Q_{ext}, the extinction efficiency, by dividing by the NW diameter (the 1-D optical

cross section). A plot of Q_{ext} vs. diameter for Ag and Cu can be found in the supporting information (FIG. S3).

Due to the insulating nature of the Cu NW native oxide shell and the electrochemically active Cu core, when a pair of Ag electrodes are put in contact with a single NW, and a sufficiently high voltage applied, resistive switching can occur at the wire-electrode interface. Cu and Ag are widely used as an oxidizable (soluble) electrode in many metal-electrolyte-metal (MEM), or metal-insulator-metal (MIM) thin-film devices.[18] Electroforming involves applying a positive voltage to the oxidizable electrode which leads to the dissolution of the metal, migration through the insulating layer and deposition of a metallic filament at the opposite electrode. As more material is deposited, a "virtual cathode" grows back through the oxide towards the anode, and ultimately bridges the two electrodes.[19] The voltage this occurs at is defined as V_{SET}, defining a low-resistance ON state (LRS). The resistance of the LRS can be set by limiting the current compliance. When the current compliance is removed, and sufficient current (I_{RESET}) is driven through the nanoscale filament in the LRS, Joule heating causes a thermal dissolution of the filament, and the conducting bridge is disconnected, establishing a high resistance OFF state (HRS) by unipolar resistive switching.[20] The junction activation process in a network of oxide coated Cu NWs has been shown to result in a winner-takes-all conducting path formation.[21] Furthermore, CuO_x NWs have demonstrated forming-free non-volatile resistive switching and memristive effects.[22] Further study is warranted on these types of materials as they could enable flexible transparent memories and multifunctional devices.

Establishing a stable low-resistance ohmic contact between the EBL-defined electrodes (FIG. 1(a)) and the Cu core requires electroforming the connections. FIG. 1(b) displays an *I-V* plot where voltage sweeps are performed at an increasing current compliance value and the LRS is not retained after the SET event. This is known as threshold switching and commonly occurs at low current compliance limits,[23] a plot of the threshold and LRS SET voltage vs. current compliance for 7 single nanowire devices and 3 nanowire junctions can be found in the supporting information (FIG. S4). In this device, with a 120 μA current compliance, the sample demonstrated a stable low-resistance (419 Ω) ohmic response. NWs which were typically put in a LRS using a current compliance of a few 100 μAs, could be resistively switched to the HRS through unipolar behavior at a current value of ~ 1mA. After each pair of electrodes had been electroformed to a LRS, the resistance of the NW was measured using the 4-probe method. High-resolution SEM allowed the measurement of the NW diameter, with the length of the device taken from the outer-

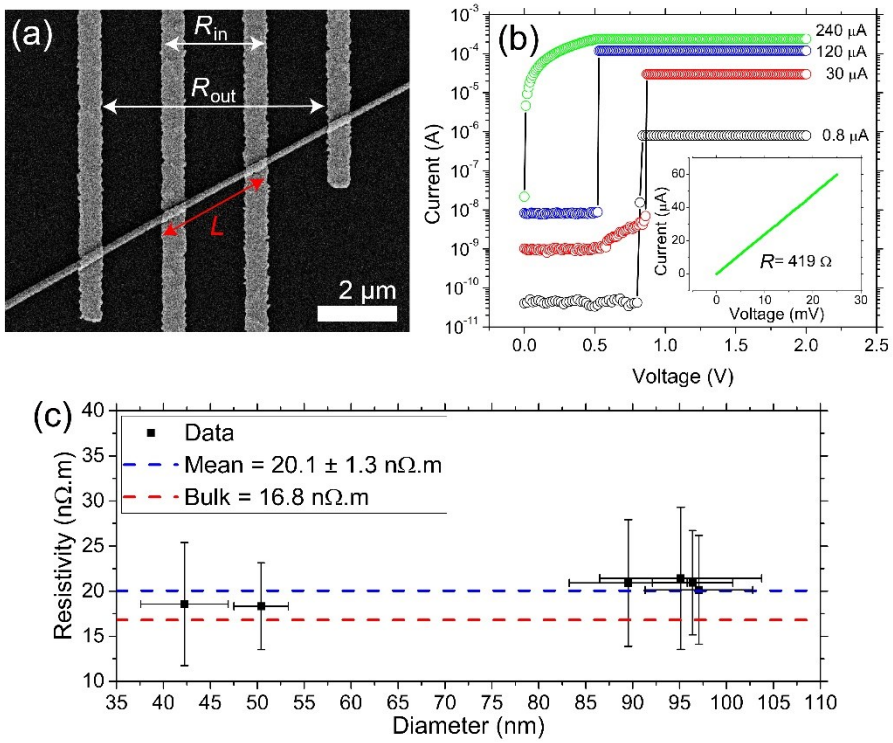

FIG. 1. Electroforming for ohmic conduction in a single Cu NW. (a) SEM image of a single Cu NW contacted with 4 electrodes for resistivity (ρ) measurements. The inner and outer electrodes are identified for the 4-probe measurement. (b) I-V curve showing the electroforming process by increasing current compliance. The inset curve shows the low resistance (419 Ω) ohmic response after electroforming. (c) ρ values for 6 individual NWs of varying diameter, with error bars originating from standard deviation of 10 measurements of the NW diameter. The ρ value for bulk Cu is shown by the red dashed line at 16.8 nΩ·m. Cu NW $\langle\rho\rangle$ is plotted by the blue dashed line at 20.1 ± 1.3 nΩ·m.

most edge of the inner two electrodes (FIG. 1(a)) when calculating the material resistivity, ρ, as per Koleśnik-Gray et al.[24]

The thickness of the native oxide was accounted for in the diameter of the NW using the linear dependence of the oxide thickness on the diameter (D) observed by TEM (FIG. S1(e)). The ρ for 6 samples was calculated and plotted in FIG. 1(c). The mean resistivity $\langle\rho\rangle$ = 20.1 ± 1.3 nΩ·m (blue dashed line) is closer to the bulk value than previously measured solution grown Cu NWs (35 nΩ·m),[7] but higher than electrodeposited and highly twinned Cu NWs (17.8 nΩ·m).[25] The bulk ρ value for Cu is shown as the red dashed line in FIG. 1(c) with a value of 16.8 nΩ·m. Compared to measurements for Ag NWs (20.3 ± 5.5 nΩ·m),[9] our results show a no appreciable difference in the conductivity of solution grown Cu NWs and Ag NWs.

Establishing the Cu NW ρ is crucial to accurately calculating the junction resistance R_{jxn}. As in the case of the single NW measurements, an electroforming procedure was run between each of the contacts (electrodes 1-2, and 3-4) to the NW either side of the junction, and then to the junction

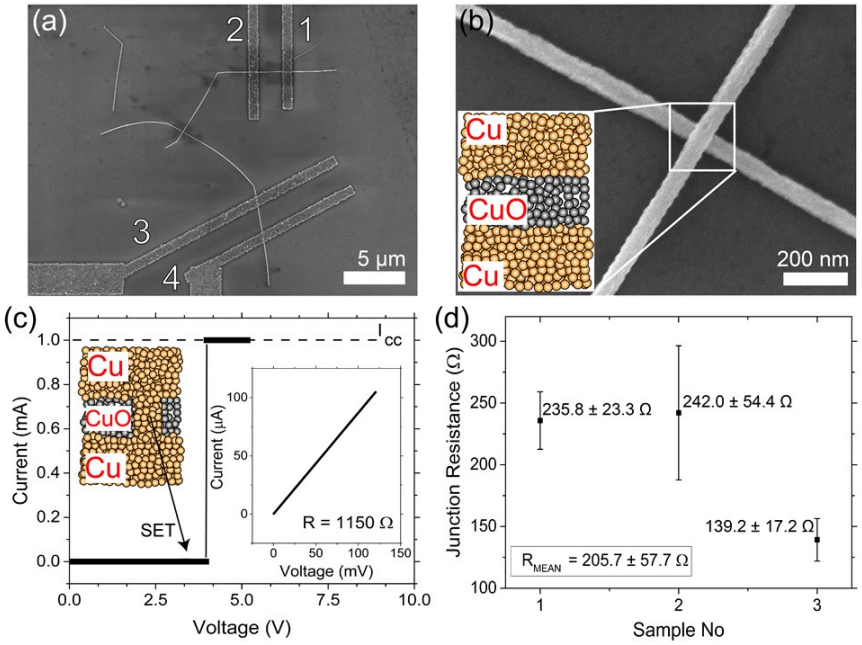

FIG. 2. Cu NW R_{jxn} measurement. (a) SEM image of a Cu NW junction contacted for 4-probe measurement. (b) Magnified SEM of the NW junction. The inset schematic illustrates the metal-insulator-metal structure of the junction in the pristine, non-conductive state. (c) Electroforming I-V curve for the NW junction, with a current compliance of 1 mA. The inset graph shows the resistance of a subsequent 2-probe measurement with a resistance of 1150 Ω. The top-left inset schematic depicts the Cu conductive bridge formed through the oxide. (d) Measurements on three individual junctions yield $\langle R_{jxn} \rangle = 205.7 \pm 57.7$ Ω.

itself (electrodes 2-3) (FIG. 2(a)). Bringing the junction into a LRS involves creating a conductive filament through both oxide shells (FIG. 2(b)).

The electroforming process is carried out in the same manner to that used in the activation of the electrical contacts on a single Cu NW. The voltage is linearly increased until a SET event occurs and the current flow across the device quickly increases until it reaches the limiting current compliance (1 mA in this case). Through this process, the device is taken from the pristine HRS to a LRS (FIG. 2(c)). The inset schematic illustrates the conductive filament, which bridges the two metallic NW cores. The inset *I-V* curve shows the 2-point ohmic response of the NW junction after electroforming with a resistance value of 1150 Ω. After a stable electrical connection is established for all the EBL-defined contacts and the junction, a 4-probe measurement of the crossed NW structure can be performed.

Removing the resistance contributions from the NW lengths up to the junction involves the same calculation as previously described for Ag NW junctions,[9] but with one difference, the oxide thickness is removed from the measured D of the NW as it does not contribute to electrical conduction. The graph shown in FIG. 2(d) shows the R_{jxn} measurements for three individual Cu

NW junctions. $\langle R_{jxn} \rangle$ was calculated to be 205.7 ± 57.7 **Ω**, significantly higher than the median value for Ag NW junctions, $\langle R_{jxnAg} \rangle$ = 11 **Ω**.[9]

We recently published a method which accurately describes the electrical and optical performance of Ag NWNs using a multi-nodal representation (MNR) of a NWN, that is, considering both the resistance contribution of the NW junctions and the NW segments between them; coupled with an optical model based on Mie light scattering theory (MLST).[11] The electrical results presented above allow the MNR and MLST model to be applied to Cu NWs, predicting the electro-optical performance of a Cu NWN transparent conductor electrode using only physical properties such as NW length (L) and diameter (D), electrical parameters such as $\langle \rho \rangle$ and $\langle R_{jxn} \rangle$, and the optical constants of Cu. By choosing physical parameters that match datasets already published in the literature, we can test the MNR and MLST model on its predictive accuracy. If the ab-initio model predicts data consistent with experimental observation, it would be a powerful tool to forecast, benchmark and design Cu NWNs for specific purpose. Furthermore, the average R_{jxn} component of the R_s can be varied to determine the efficacies of post-processing techniques, synthesis methods, deposition procedures and to assess the ultimate performance of the NWN as $R_{jxn} \rightarrow 0$.

FIG. 3 displays the experimental and computationally predicted datasets of four Cu NWN systems with aspect ratios (AR) ranging from 330 to 1860. For each set of simulations, L and D values were set to match the NW dimensions reported by the authors in the experimental measurements. Simulations were performed with three values of $\langle R_{jxn} \rangle$, 205 **Ω**, representing the average R_{jxn} measured in this work, 100 **Ω**, and a "highly optimized" $\langle R_{jxn} \rangle$ value of 1 **Ω**. These $\langle R_{jxn} \rangle$ values are plotted in red, blue and green, respectively. FIG. 3(a-b) presents the experimental results of Borchert *et al*. where Cu NWs with an AR of 330 and 570, respectively, were dispersed in a nitrocellulose-based ink and printed onto PET (Polyethylene terephthalate) using a Meyer rod. The films were subjected to a 4x repeated rinsing in acetic acid to improve the R_s. The authors used a Monte-Carlo model which approximates that R_s originates from R_{jxn} only and included a L dispersity to fit experimental data. Through this method they extracted a lower boundary for R_{jxn} = ~2 k**Ω**, and an upper boundary R_{jxn} = ~10 k**Ω** with no modeling of the optical properties.[13] The MNR and MLST model predicts the R_s and T of the networks with close agreement to the experimental data in the case of AR = 330, slightly overpredicting the performance for AR = 570. FIG. 3(c-d) displays the experimental data from Ye *et al.* who fabricated Cu NWs of AR = 460 and 1860, respectively. For larger aspect ratio systems, the T exhibits less dependence on R_{jxn}.

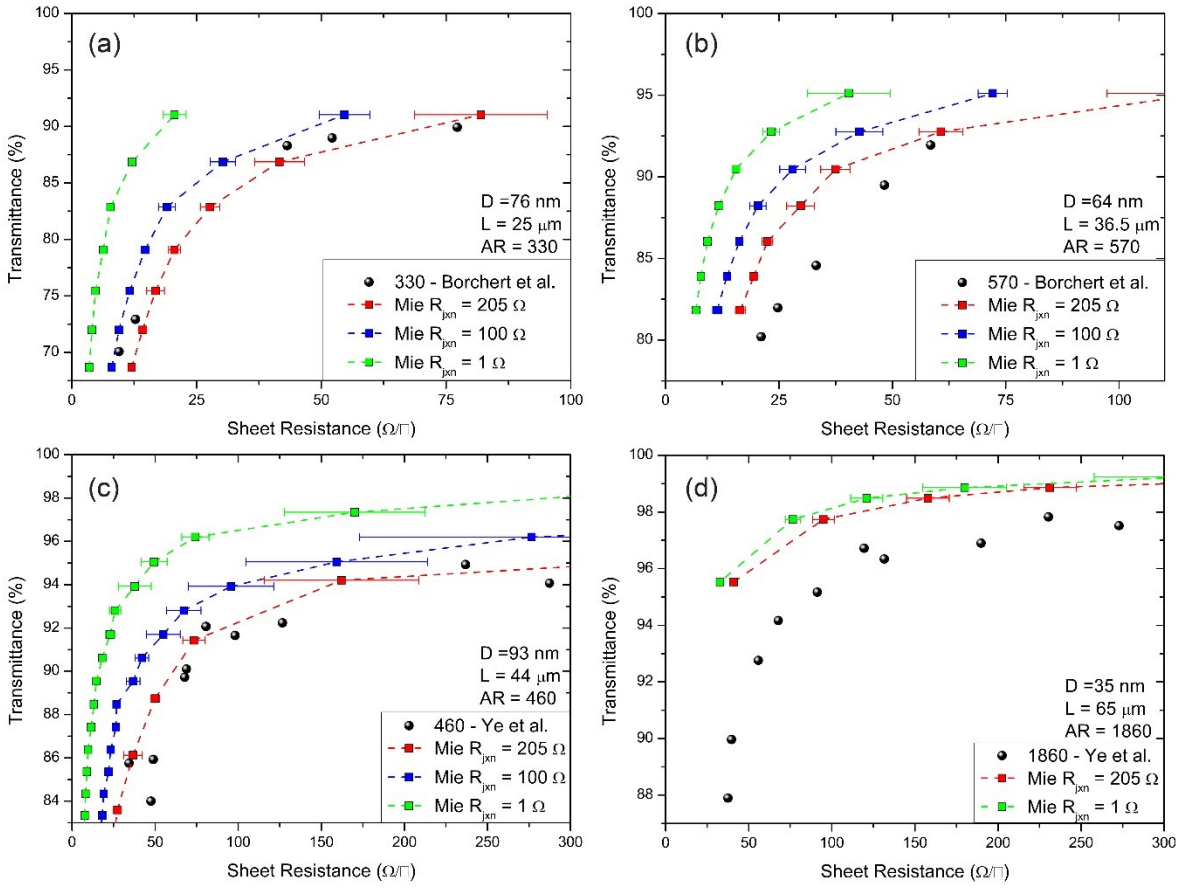

FIG. 3. Transmittance vs. sheet resistance, experimental, and simulated predictions for four datasets of Cu NWNs. (a-d) The black circular points on each panel represent experimental data of Cu NWNs from reported literature values, the diameter (D), length (L) and aspect ratio (AR = L/D) for each dataset detailed on the right of each graph.[8,13] The colored square datapoints show the predictions of the MNR and MLST model where, in red, R_{jxn} = 205 Ω, in blue R_{jxn} = 100 Ω, and in green R_{jxn} = 1 Ω. The error bars at each of the simulation datapoints show the standard deviation of the R_s for 10 simulated networks samples.

This is due to a decrease of junction density with increasing L,[12] and a reduction of Q_{ext} with decreasing D. All Cu NWN films were deposited by Meyer rod coating, plasma cleaned and annealed in a tube furnace for 30 minutes at 225 °C.[8] The computational results match the experimental measurements throughout the R_s range for AR = 460, and slightly overpredicts the performance of the network for AR = 1860 by < 4 % T. The discrepancy could be accounted for by adding more complexity to the MNR model, considering NW curviness and distributions of L, D and R_{jxn} values, none of which are accounted for in the present model. A further dataset using NWs of AR = 384 where the model overestimates the performance of the NWN can be found in the supporting information (FIG. S5)

The shape of the experimentally acquired T-R_s curve is also important, as networks which are not fully optimized through post-processing can exhibit abnormal T-R_s profiles that deviate from the

standard shape, and which the MNR and MLST model can highlight.[11] In all cases reported here, the MNR and MLST model utilizing a $\langle R_{jxn} \rangle = 205\ \Omega$ accurately predicts the performance of real world networks. This indicates that the high-current electroforming process employed in the measurement of the single NW junctions in this work reproduces a R_{jxn} comparable to the post-processing methods employed in the fabrication of Cu NWNs.

In conclusion, we report the electrical properties of single and crossed solution-grown Cu NWs. While the material resistivity $\langle \rho \rangle$ for the Cu NWs of 20.1 ± 1.3 nΩ·m was comparable to that of Ag NWs, the resistance of electroformed junctions $\langle R_{jxn} \rangle$ was measured to be almost 20x larger at 205.7 ± 57.7 Ω. Electrical characterization of individual Cu NWs enabled the electro-optical modeling of Cu NWNs, which accurately predicts the electrical and optical performance of real Cu NWNs based on physical parameters and optical constants only. These results represent a further step towards a materials-by-design approach for NWNs, investigating the fundamental material properties of individual NWs to chase the limits of performance for a collective network. We hope this work will motivate and inform the search for processing technologies and alternate NW materials that reduce cost, environmental burden and see the full potential of NWN-based technologies realized.

Supplementary Material

See the supplementary material for SEM and TEM images of the Cu NWs used in the study including L and D distributions. A graph of the native oxide thickness with respect to NW D. Threshold and LRS SET voltages vs. current compliance. A plot of Q_{ext} vs. NW D for Cu and Ag. MNR and MLST data with good agreement for NWN systems with AR = 384.

Acknowledgements

The authors wish to acknowledge funding from the European Research Council (ERC) under Advanced grant 321160. This publication has emanated from research supported by grants from Science Foundation Ireland (SFI) under P.I grant 16/IA/4462, 18/IF/6324 and the SFI Research Centre, AMBER under grant number 12/RC/2278. The facilities and staff at the Advanced Microscopy Laboratory at Trinity College Dublin are greatly acknowledged for their support. The authors also acknowledge the Research IT Unit (formerly TCHPC) at Trinity College Dublin and the WestGrid (www.westgrid.ca) and Compute Canada Calcul Canada (www.computecanada.ca) for computational resources.

Author Contributions

H.G.M. wrote the paper, performed the electrical measurements and the MNR and MLST simulations. P.F.F and M.A.C., led by B.J.W. synthesized the Cu NWs. C.G.R. and C. O'C., led by M.S.F. developed the MNR computational model. J.J.B. led overall effort. All authors discussed and commented on the manuscript and on the results.

The authors declare no competing financial interest.

The data that support the findings of this study are available from the corresponding author upon reasonable request.

References

[1] D. Bellet, M. Lagrange, T. Sannicolo, S. Aghazadehchors, V. H. Nguyen, D. P. Langley, D. Munoz-Rojas, C. Jimenez, Y. Brechet, and N. D. Nguyen, Materials (Basel) **10** (6), 570 (2017).

[2] S. Ye, A. R. Rathmell, Z. Chen, I. E. Stewart, and B. J. Wiley, Adv Mater **26** (39), 6670 (2014).

[3] C. G. Rocha, H. G. Manning, C. O'Callaghan, C. Ritter, A. T. Bellew, J. J. Boland, and M. S. Ferreira, Nanoscale **7** (30), 13011 (2015).

[4] I. E. Stewart, A. R. Rathmell, L. Yan, S. Ye, P. F. Flowers, W. You, and B. J. Wiley, Nanoscale **6** (11), 5980 (2014).

[5] U. S. Geological Survey, *Mineral Commodity Summaries*. (2019).

[6] Y. Wang and Z. Yin, Applied Science and Convergence Technology **28** (6), 186 (2019).

[7] W.-H. Xu, L. Wang, Z. Guo, X. Chen, J. Liu, and X.-J. Huang, ACS nano **9** (1), 241 (2014).

[8] S. Ye, A. R. Rathmell, I. E. Stewart, Y. C. Ha, A. R. Wilson, Z. Chen, and B. J. Wiley, Chem Commun (Camb) **50** (20), 2562 (2014).

[9] A. T. Bellew, H. G. Manning, C. G. Rocha, M. S. Ferreira, and J. J. Boland, ACS Nano **9** (11), 11422 (2015).

[10] F. Selzer, C. Floresca, D. Kneppe, L. Bormann, C. Sachse, N. Weiß, A. Eychmüller, A. Amassian, L. Müller-Meskamp, and K. Leo, Applied Physics Letters **108** (16), 163302 (2016).

[11] H. G. Manning, C. G. Rocha, C. O. Callaghan, M. S. Ferreira, and J. J. Boland, Sci Rep-Uk **9** (1), 11550 (2019).

[12] C. O'Callaghan, C. G. Rocha, H. G. Manning, J. J. Boland, and M. S. Ferreira, Phys Chem Chem Phys **18** (39), 27564 (2016).

[13] J. W. Borchert, I. E. Stewart, S. Ye, A. R. Rathmell, B. J. Wiley, and K. I. Winey, Nanoscale **7** (34), 14496 (2015).

[14] K. Mallikarjuna, H.-J. Hwang, W.-H. Chung, and H.-S. Kim, RSC Advances **6** (6), 4770 (2016).

[15] A. R. Rathmell and B. J. Wiley, Adv Mater **23** (41), 4798 (2011).

[16] J. Schäfer, S. C. Lee, and A. Kienle, Journal of Quantitative Spectroscopy and Radiative Transfer **113** (16), 2113 (2012).

[17] P. B. Johnson and R. W. Christy, Physical Review B **6** (12), 4370 (1972).

[18] I. Valov and M. N. Kozicki, Journal of Physics D: Applied Physics **46** (7), 074005 (2013).

[19] H. G. Manning, S. Biswas, J. D. Holmes, and J. J. Boland, ACS Appl Mater Interfaces **9** (44), 38959 (2017).

[20] R. Waser and M. Aono, Nat Mater **6** (11), 833 (2007).

[21] H. G. Manning, F. Niosi, C. G. Rocha, A. T. Bellew, C. O'Callaghan, S. Biswas, P. F. Flowers, B. J. Wiley, J. D. Holmes, M. S. Ferreira, and J. J. Boland, Nat Commun **9** (1), 3219 (2018).

[22] K. D. Liang, C. H. Huang, C. C. Lai, J. S. Huang, H. W. Tsai, Y. C. Wang, Y. C. Shih, M. T. Chang, S. C. Lo, and Y. L. Chueh, ACS Appl Mater Interfaces **6** (19), 16537 (2014).

[23] R. Waser, R. Dittmann, G. Staikov, and K. Szot, Advanced materials **21** (25-26), 2632 (2009).

[24] M. M. Koleśnik, S. Hansel, T. Lutz, N. Kinahan, M. Boese, and V. Krstić, Small **7** (20), 2873 (2011).

[25] S. Zhong, T. Koch, M. Wang, T. Scherer, S. Walheim, H. Hahn, and T. Schimmel, Small **5** (20), 2265 (2009).

Supplementary Information:
The Resistance of Cu Nanowire-Nanowire Junctions & Electro-Optical Modeling of Cu Nanowire Networks

Hugh G. Manning,[1,2, a)] Patrick F. Flowers,[3] Mutya A. Cruz,[3] Claudia Gomes da Rocha,[4] Colin O' Callaghan,[5] Mauro S. Ferreira,[2,5] Benjamin J. Wiley,[3] and John J. Boland [1,2]

[1] *School of Chemistry, Trinity College Dublin, Dublin 2, Ireland.*

[2] *Advanced Materials and Bioengineering Research (AMBER) Centre, Trinity College Dublin, Dublin 2, Ireland.*

[3] *Department of Chemistry, Duke University, Durham, North Carolina, NC 27708-0354, USA.*

[4] *Department of Physics and Astronomy, University of Calgary,2500 University Drive NW, Alberta T2N 1N4, Canada.*

[5] *School of Physics, Trinity College Dublin, Dublin 2, Ireland.*

[a)] Author to whom correspondence should be addressed. Electronic mail: manninh@tcd.ie

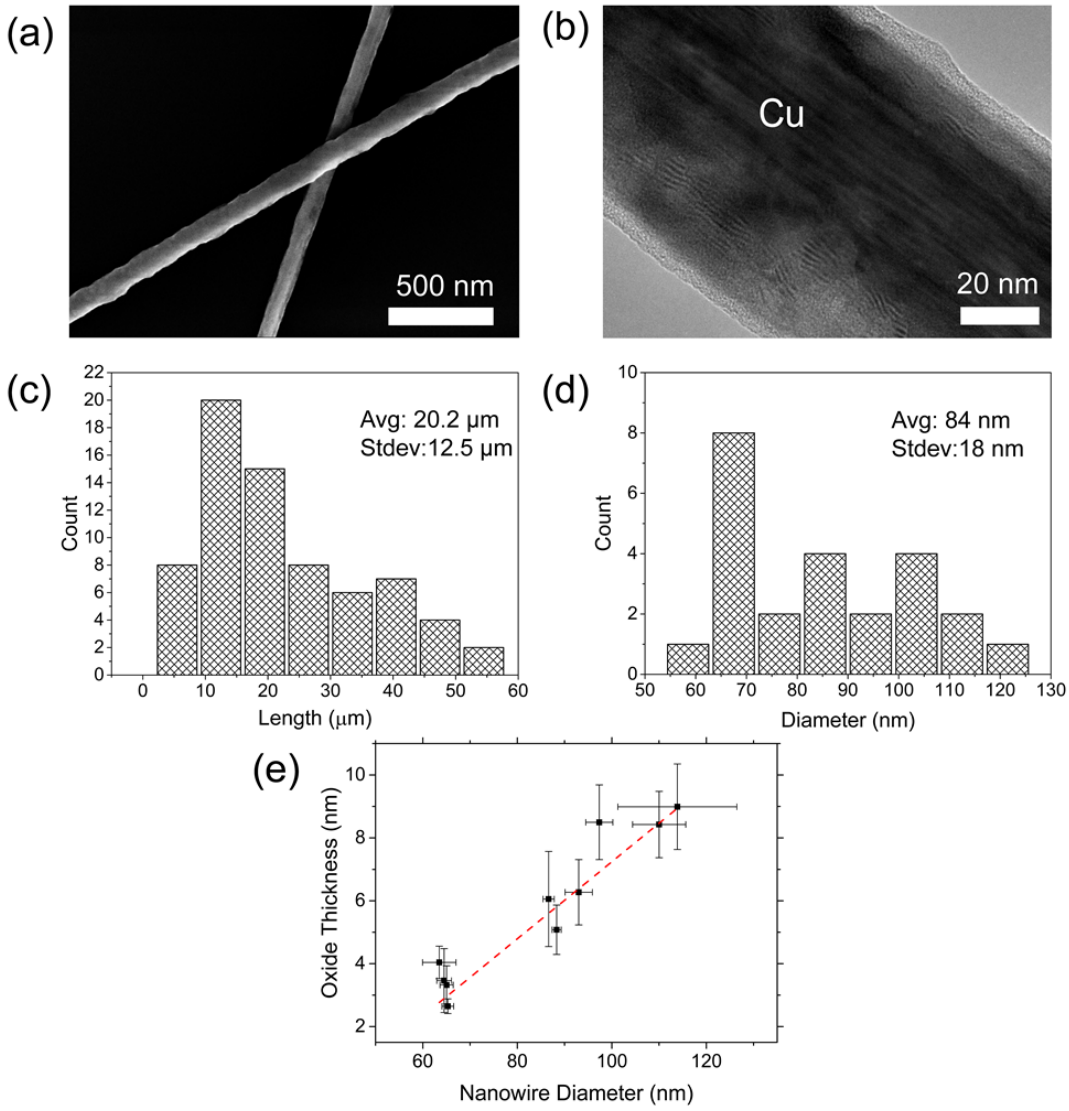

FIG. S1. Characterization of Cu nanowires. (a) Scanning electron microscope image of two overlapping Cu nanowires drop cast onto a SiO_2 substrate. (b) High resolution transmission electron microscope (TEM) image of a Cu nanowire with a thin native oxide coating the surface. (c) and (d) show length and diameter distributions of the batch of Cu nanowires used for single nanowire and junction resistance measurements in the main manuscript. Intrinsic surface roughness, and device to device variation is pervasive in these types of solution grown nanowires. We estimate the surface roughness from the SEM and TEM images is < 10 nm. (e) From TEM inspection a correlation between native oxide thickness with respect to nanowire diameter is shown, errors are generated from the 10 measurements performed on each wire, the red line is a linear fit to the data.

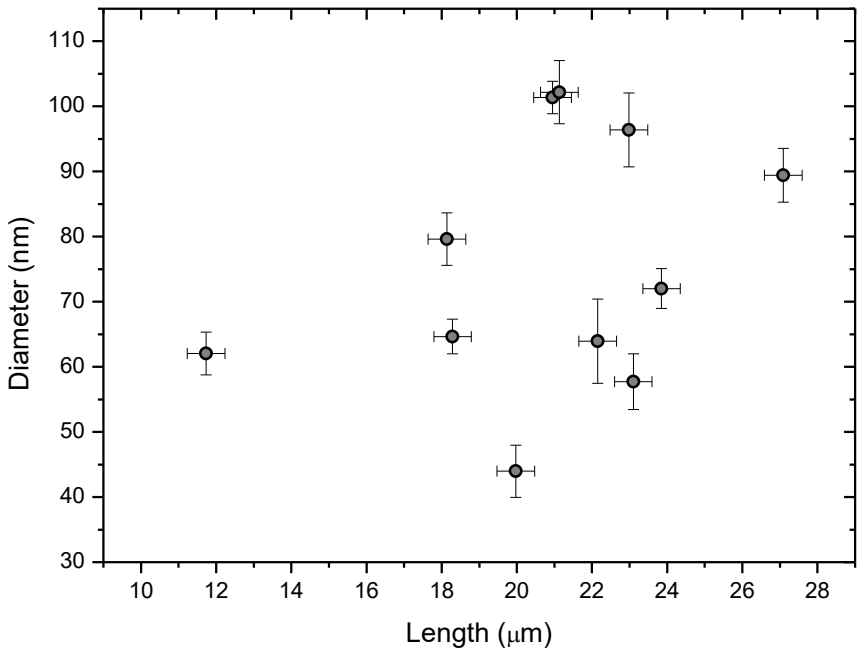

FIG. S2. Characterization of Cu nanowires from scanning electron microscope imaging. No significant correlation was found between the nanowire length and diameter.

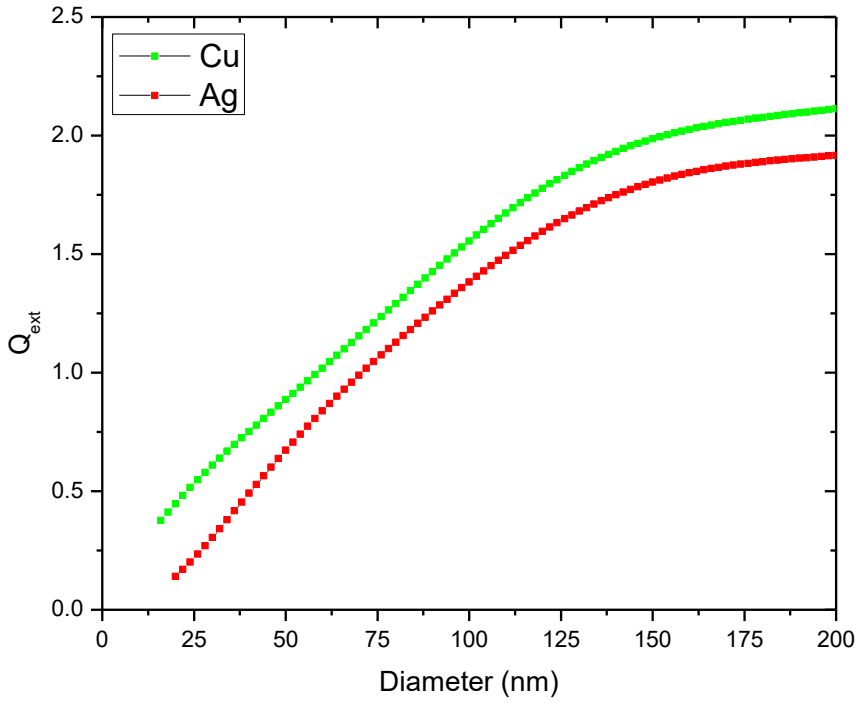

FIG. S3. Q_{ext} vs. nanowire diameter for Cu and Ag, calculated using MatScat[1] for a single infinite circular cylinder.

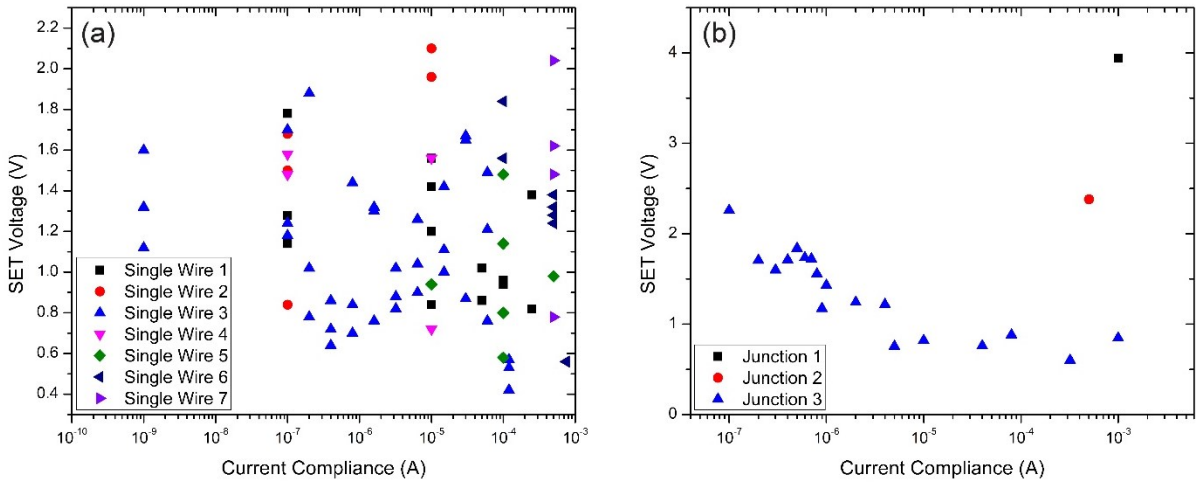

FIG. S4. The threshold and low resistance state SET voltage for a range of current compliance limits for (a) 7 single nanowires and (b) 3 nanowire junctions. Multiple measurements were made on the same nanowire devices, at large current compliances devices achieved a stable low resistance state. (a) No trend was observed between the current compliance and the SET voltage, the spread of activation voltages across the 7 samples is likely caused by device to device variation, changes in nanowire diameter, oxide thickness and surface roughness, the electrode separation was 2 µm on all samples. (b) Junctions 1 and 2 were activated to a current compliance of 1 mA and 500 µA, respectively. Junction 2 was activated to 1 mA in a subsequent measurement but there was a gradual increase of current and not a sharp transition. Junction 3 was activated slowly by increasing the current compliance limit on each *I-V* sweep. As the current compliance is gradually increased the conductive filament between the nanowires partially forms and the threshold SET voltage plateaus ~700 mV.

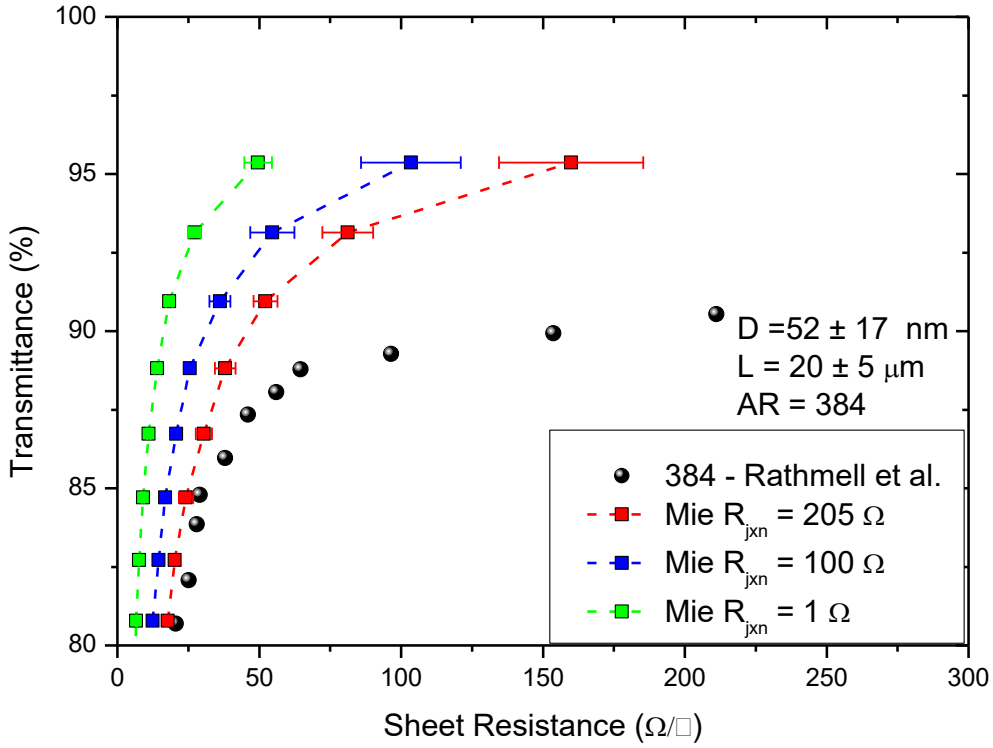

FIG. S5. Transmittance (T) vs. sheet resistance (R_s), experimental, and simulated predictions for Cu nanowire networks (NWNs) of AR 384. The black circular points represent experimental data of Cu NWNs from Rathmell *et al.*,[2] the diameter (D), length (L) and aspect ratio (AR = L/D) are detailed on the right of each graph. These Cu NWNs were dispersed in a nitrocellulose-based ink and Meyer Rod coated onto PET. The films were then plasma cleaned in a forming gas atmosphere and subsequently annealed in a tube furnace with a pure H atmosphere at 175 °C. The colored square datapoints show the predictions of the MNR and MLST model where, in red, R_{jxn} = 205 Ω. The error bars at each of the simulation datapoints show the standard deviation of the R_s for 10 simulated networks samples. For sparse networks there is a small divergence (~ 5 %) between the T of the experimental and simulation data, the divergence in T cannot be accounted for by simply increasing R_{jxn} as that can only impact the electrical performance shifting the simulated data further to the right and improving the fit of the first 5 datapoints only (4 of which are already within ~10 Ω when R_{jxn} = 205 Ω). Increasing R_{jxn} will not shift the simulated curves downward which would be necessary to align with the rest of the datapoints. A downward transformation could be induced by incorporating into the simulation model the distribution of L and D in the experimental nanowires, taking into account debris/impurities in the experimental network which would serve to reduce transmittance but not contribute to the electrical performance.

REFERENCES

[1] J. Schäfer, S. C. Lee, and A. Kienle, Journal of Quantitative Spectroscopy and Radiative Transfer **113** (16), 2113 (2012).

[2] A. R. Rathmell and B. J. Wiley, Adv Mater **23** (41), 4798 (2011).